BINOCULAR IMAGING WITH THE CONFORMAL EYES

Jacek Turski*
Department of Mathematics and Statistics
University of Houston-Downtown
Houston, TX 77002
turskij@gmail.com

June 6, 2022

ABSTRACT

The human eye possesses a natural asymmetry of its optical components and an inhomogeneous distribution of photoreceptors causing optical aberrations and providing high acuity only at a 2-degree visual angle. Although these features greatly impact the visual system functions, they have not been supported by the geometric formulation of the fundamental binocular concepts. The author recently constructed a geometric theory of the binocular system with asymmetric eyes (AEs) integrated with the eyes' movement to address these problems. This theory suggests that a symmetric framework can fully represent the asymmetric properties of this binocular system with the AEs. Pursuing this idea leads to the conformal eye model furnished by the Riemann sphere. The conformal geometry of the Riemann sphere establishes efficient image representation in terms of the projective Fourier transform (PFT)—the Fourier transform on the group of image projective transformations representing images covariantly to these transformations. The PFT is fast computable by an FFT algorithm in log-polar coordinates known to approximate the retina-cortical mapping of the human brain's visual pathways. The retinotopy modeling here with PFT is compared to Schwartz's modeling with the exponential chirp transform showing clear advantages of PFT in both physiological conformity and numerical efficacy. Finally, the conformal eye model is extended to the AE, which can be implemented into the binocular system with AEs making PFT available for image processing. The PFT combined with the conformal eye model allows binocular extensions of the previous monocular algorithms for modeling visual stability during the saccade and smooth pursuit eye movements needed to offset the eye's acuity limitation.

Keywords Asymmetric eye · Riemann sphere · Conformal geometry · Conformal eye · Fourier analysis on groups · Projective Fourier transform · Retinotopy

1 Introduction

The human eye is an optical system comprising the cornea, the crystalline lens, and the nonuniform light-sensitive retina with a high acuity fovea limited to a two-degree visual angle. The human eye has an imperfect optical design: the fovea's temporalward displacement from the posterior pole produces the eyeball's global asymmetry, and the lens is tilted relative to the cornea. The fovea's displacement and the asphericity of corneal surfaces are the main sources of optical aberrations. The lens' tilt and distribution of the gradient refractive index, on the other hand, are part of the eye's aplanatic design that produces nearly aberration-free perception near the visual axis [3, 34]. However, the two eyes working in unison in the binocular system improve visual acuity and assist visually guided tasks with precise eye movements [16, 47].

Because our two eyes are separated laterally in the head, they receive two-dimensional disparate projections of the world. Despite this disparity, we usually perceive one world with the impression of stereoscopic depth. The basic concepts underlying binocular vision and stereopsis are retinal correspondence and horopter. For a given binocular fixation,

*Professor emeritus

the horopter is the locus of points in space such that each point on the horopter projects to a pair of corresponding retinal elements, one in each eye. Each pair of corresponding elements is distinguished by the quality of seeing a small object that projects onto them in a specific but subjective direction. We say that the corresponding elements have zero disparity.

Normal correspondence occurs when the fovea of one eye corresponds to the fovea of the other eye; their single visual direction is called the principal visual direction, or the Cyclopean direction. The visual directions of all other pairs of stimulated corresponding elements are perceived relative to this principal direction, the hallmark of a single binocular vision. Points far from the horopter are projected on noncorresponding elements such that they have non-zero disparity and are generally seen as double.

However, each point in the so-called Panum's fusional region around the horopter is seen as single. Then, the brain uses the extracted disparity to create our sense of depth relative to the horopter. Further, the disparity between two spatial points in the Panum's area provides us with stereopsis–the ability to perceive form. Even objects far from the horopter curve that we see double provide the sense of depth [23], which gives us the spatial order of objects and, hence, the phenomenal space geometry.

The author developed two binocular systems, each with a more advanced fidelity of eye model. In the reduced eye model, the eye optics is represented by one refractive spherical surface with the nodal point at its curvature center and the fovea at the posterior pole. The nodal point and the fovea located on the optical axis define the eye's axial symmetry. The nodal point is located 0.6 cm anterior to the eye's rotation center. The image on the retina is impinged by the pencil of light rays based at the nodal point.

This symmetric eye (SE) model was used in [40] to correct the 200-year-old Vieth-Müller circle (VMC) model of the geometric horopter that is still used today in research and education. The analytic form of the VMC has been known for an arbitrary fixation only when the nodal point is placed incorrectly in the eye's rotation center. In this case, when the eyes' are fixating on points on the VMC, it remains stationary. Otherwise, the VMC has only been known for symmetric fixations for all other nodal point locations. In [40], the analytical form of the geometric horopter when the eye's nodal point is anatomically located was given for arbitrary horizontal bifoveal fixations for the first time. The relative disparity was in the range of binocular acuity, and its significance for fine aspects of binocular perception was discussed.

The asymmetric eye (AE) model is introduced and comprehensively discussed in [43] and slightly modified in [44]. It extends the reduced eye with the eye's natural misalignment of human optics. The AE is comprised of the fovea's anatomical displacement from the posterior pole by angle $\alpha = 5.2^\circ$ and the crystalline lens' tilt relative to the cornea by angle β. Angle α is relatively stable in the human population, and angle β varies between -0.4° and 4.6°. In the human eye, the fovea's displacement from the posterior pole and the cornea's asphericity contribute to optical aberrations that the lens' tilt then partially compensates for [Artal 2014]. Further, a geometric theory of the binocular system with the AEs' developed in [44] in the framework of bicentric perspective projections advanced the work by Ogle [22] and Amigo [2] on modeling empirical horopters as conic sections. In contrast with their theory, the biologically supported horopteric conics in [44] pass through the nodal points, are integrated with eye movement, and their geometric transformations during eye movements are visualized in a computer simulation.

When eyes are binocularly fixated straight ahead such that the image planes of the AEs, defined as parallel to the lens's equatorial planes and passing through the eye's center, are coplanar, the constructed horopter is a straight frontal line parallel to the image planes; see Figure 4 in [44]. The distance to this fixation point is called the abathic distance explicitly given in this reference in terms of the ocular separation and the AE's parameters α and β. This case of linear horopter proves that the unequal distribution of retinal corresponding points for asymmetric eyes can be defined in terms of the image plane's symmetrical distribution of projected retinal points into the plane [44]. This geometric result suggests that one can fully dispense with the spherical retina in the AE.

To do this, however, I need to show that the receptive fields on the circular retina—the units of neural circuits processing visual information— are preserved to a large degree when projected into the image plane and, hence, the retinal illuminance is also preserved. The consequences of this property will take us well beyond concepts typically associated with the horopter.

The paper is organized as follows. I first discuss the SE model, that is, the AE with $\alpha = \beta = 0$, emphasizing the geometric properties of the projection of the retina onto the image plane for three different locations of the nodal point: the pupil identified with the north pole of the unit sphere, the approximate anatomical location of 0.6 cm anterior the eye's rotation center and the rotation center. The nodal point can be depicted in publications in any of these locations but is located most often at the rotation center, especially in vision sciences computational study; see [28] for example.

The north pole location of the nodal point is distinguished for providing anatomically acceptable numerical approximation and efficient tools for image processing. In particular, the projection from the retina to the image plane is the

conformal stereographic mapping: it preserves under the projection the angle of the two intersecting curves. It also maps circles in the retina that do not contain the north pole to circles in the image plane. Thus, stereographic mapping preserves receptive fields and retinal illuminance such that the image plane can faithfully represent the retina.

I will explain later that the nodal point placed at the north pole preserves the qualitative properties of the anatomically correct location of the nodal point with a very good numerical approximation for the anthropomorphic binocular system's parameters. On the other hand, when the nodal point is placed at the eye's rotation center, the eye model degenerates binocular geometry even though the numerical approximation is good.

Because stereographic mapping is not defined at the nodal point identified with the north pole, it is extended one-to-one and onto by appending to the image plane the point at infinity, which is the image of the nodal point under this mapping. The image plane with the appended point at infinity is the celebrated object in geometry, and mathematical analysis is known as the Riemann sphere [21]. Thus, the SE with the extended image plane that substitutes for the retina is given by the Riemann sphere—the newest and most compelling eye model referred to as the conformal eye (CE).

The Riemann sphere's conformal geometry identifies the structure of the one-dimensional complex projective geometry [6] with the Möbius geometry [14]. This identification means the group of image projective transformations resulting from the change of perspective between the scene and the eye's orientation agrees with the group of Möbius transformations. The CE provides a unique geometric environment that is relevant to the intermediate-level vision computational aspects of natural scene understanding [39, 41].

Further, the Riemann sphere's conformal geometry establishes image representation in terms of the projective Fourier transform constructed in the noncompact picture of the Fourier analysis on the semisimple group $\mathbf{SL}(2,\mathbb{C})$ of image projective transformations [36, 37]. This image representation changes covariantly with the image transformations induced by eye rotations. It is fast computable by FFT in log-polar coordinates that are known to approximate the retina-cortical mapping of the human brain's visual pathways [38, 41]. Although the CE model is introduced and discussed for the SE model, in the last section, it is extended to the AEs.

2 The Conformal Geometry in Imaging

The geometric theory in [44] shows that the non-symmetrical distribution of the corresponding retinal elements, determined by the asymmetry parameters of the AE, can be fully formulated in terms of the symmetrical distribution of their projection points in the image plane. This relationship is established by the image planes being coplanar for fixations at the abathic distance that implies the horopter through the fixation point a straight line parallel to the image planes. This fact suggests that the nodal point and the image plane can fully specify the AE model.

However, to fully dispense with the retina in the AE model, I need to show that the receptive fields and retinal illuminance are preserved under the projection from the retina to the image plane. This simple requirement will take us in the remaining part of the paper on a much longer journey through sophisticated mathematics that has striking relevance to retino-cortical image processing. Moreover, it can provide algorithms for visual stability in anthropomorphic vision systems of mobile robots.

2.1 The Nodal Point Location and Geometry of the Image Plane

Before discussing the geometries of idealized eye models and their implication for processing visual information, I introduce a SE model that includes some additional anatomical details shown in Figure 1.

The retina is represented by its projection from the nodal point to the image plane perpendicular to the optical axis and passing through the center C. The nodal point N is located 0.6 cm anterior to the eye's rotation center C as required by the eye's anatomy. The retina's sensory layer extends below the ora serrata line, which divides it from the non-sensory layer. The ray through N and point K on the circle at the upper boundary of the non-sensory layer is parallel to the image plane. This upper boundary connects to the zonule—the fiber band attached to the lens that changes its curvature during accommodation. The projections through N of the circles on the retina representing receptive fields below the ora serrata are ellipses in the image plane. The ratios of the ellipses axes in the image plane region subtended by visual angle of 110° at the nodal point varies from 0.7 at the high eccentricity to 1 at the foveal region. Details of the calculations are presented in Appendix A.

Two projections from a sphere to a plane define two different projective geometries. The first projection, shown in Figure 2 (A), is the stereographic projection from the north pole N to the plane that passes through the sphere's center C and is perpendicular to the line through N and C. Stereographic projection is ubiquitous in physics and mathematics and has been used for millennia in making maps. Even to mapmakers, it was well known that stereographic projection is conformal, i.e., it preserves angles of intersecting curves. Further, it maps circles in the sphere that do not contain

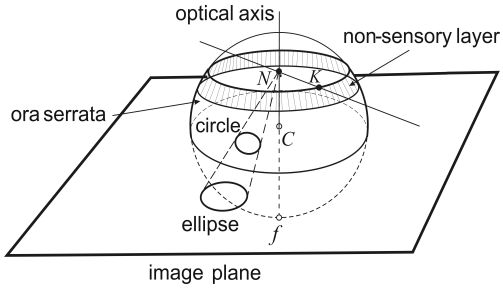

Figure 1: Figure 1: The SE model shows the non-sensory layer separated from the rest of the retina by the ora serrata. The image plane is perpendicular to the optical axis and passes through C. An ellipse is a circle on the retina below the ora serrata projected into the image plane. The nodal point N is located 0.6 cm anterior to the rotation center C at the level of the upper boundary of the non-sensory layer.

N to circles in the image plane, while any circle containing N projects onto a straight line. The plane is extended by the stereographic image of N, with the topology extended by the complement of the compact sets in the plane. The extended plane with the stereographic image of N, referred to as the point at infinity, is the Riemann sphere. The resulting conformal geometry of the extended plane with its remarkable features is carefully discussed in the next sections.

Equally important in physics and mathematics is the sphere's gnomonic, or central, projection from its center C to the plane tangent in the south pole S, shown in Figure 2 (B). The real projective plane is obtained when (1) the line at infinity is appended to the plane as the image of the sphere's equator under the projection and (2) the sphere's diagonal points are identified to make the projection one-to-one. Under the gnomonic projection, a circle on the sphere that does not intersect the equator is mapped to an ellipse. Otherwise, a tangent circle to the equator is mapped to a parabola (shown). In contrast, a circle intersecting the equator in two points is mapped to a hyperbola (not shown)—finally, the great circles other than the equator project onto straight lines.

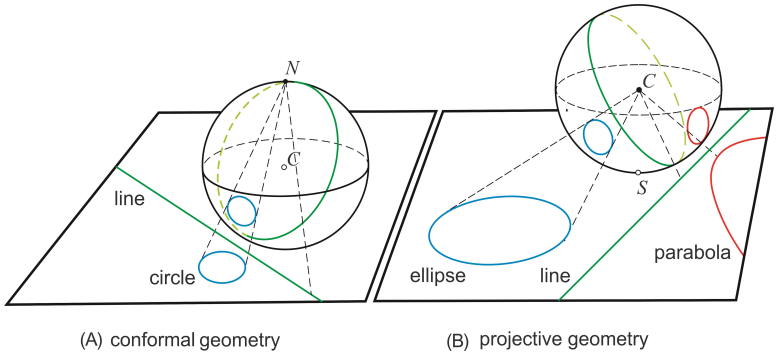

Figure 2: The two geometries are defined by projections of a unit sphere to the plane. (A) Conformal geometry of the unit sphere's stereographic projection from the north pole N to the horizontal plane passing through the sphere's center. A circle on the sphere that does not contain N projects to a circle in the plane, while a circle containing N projects onto a straight line. (B) Real projective geometry of the gnomonic projection from the center C. A tangent circle to the equator is mapped to a parabola (shown), while a circle intersecting the equator in two points is mapped to a hyperbola (not shown). The great circles other than the equator project onto straight lines.

Both projections discussed above are related to the two eye models that were used in [40] to study geometric horopters. The stereographic projection corresponds to the nodal point identified with the eye's pupil, while the gnomonic projection corresponds to the nodal point identified with the eye's rotation center. The results in [40], where the geometric horopters were studied for any location of the nodal point between the eye's pupil and rotation center, show good numerical approximations of disparities near the fixation point. However, only the family of horopters for the nodal point at the pupil retains qualitative properties of the family of horopters for the anatomically correct location of the nodal point because, in both cases, the relative disparity depends on eye movements. On the other hand, the family of horopters for the nodal point at the eye's rotation center degenerates to the family of VMCs. Because for VMCs, the relative disparity is independent of eye movements, the finest aspects of binocular vision are lost [40].

2.2 The Conformal Eye Model

The stereographic projection is shown in Figure 2 (A), denoted here by σ is not defined at the nodal point. It is extended to one-to-one and onto mapping by appending $\sigma(N)$ to the image plane. This additional point is usually denoted by ∞ and called the point at infinity. The image plane, denoted by $\mathbb{C}$, is the Gaussian plane with points (x_1, x_2) identified with complex numbers $z = x_1 + ix_2$. The extended image plane, $\widehat{\mathbb{C}} = \mathbb{C} \cup \{\infty\}$, identified with the spherical retina by stereographic projection, is the celebrated object in geometry and mathematical analysis known as the Riemann sphere, [21]. The Riemann sphere is shown in Figure 3. Stereographic projection is conformal; it preserves the angle of two intersecting curves. Further, it maps circles in the spherical retina that do not contain the nodal point to circles in the image plane, while any circle containing the nodal point projects to a straight line.

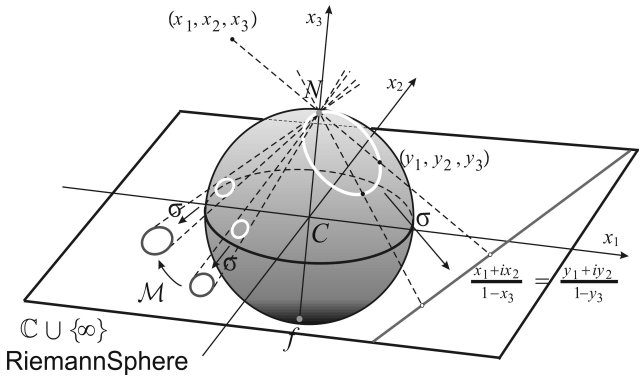

Figure 3: The Riemann sphere. The spatial points are projected through the sphere's north pole N to the sphere and the plane. Stereographic projection σ maps circles in the sphere that are not passing through N to circles in the plane. For any two circles in the plane, there is the Möbius transformation, $\mathcal{M}$, that maps one circle onto the other. A circle that contains N is projected by σ to a line. Lines are regarded as circles passing through ∞.

We note that the sphere's conformal projection to the plane, already known to Hipparchus in about 130 BC, was first named "stereographic" in 1613 by Aguilonius in *Six Books of Optics Useful for Philosophers and Mathematicians,* the treaties in which he named horopter as well.

When the eye rotates about the eyeball center to change its gaze, simultaneously, the gaze rotates at the nodal point by the same amount, and the nodal point translates. The resulting transformation on the image plane can be decomposed into two components: (1) the translation of the image out of the image plane and stereographically projected back to the image plane and (2) stereographic projection of the image on the sphere, rotating it with the sphere, and stereographically projecting back to the image plane [35, 36, 37]. Then, as it is demonstrated in these references, the finite iterations of the transformations (1) and (2) induce the group $\mathbf{SL}(2, \mathbb{C})$ of 2×2 complex matrices of determinant 1 action on the image plane by linear-fractional mappings,

$$\mathbf{SL}(2, \mathbb{C}) \ni g = \begin{bmatrix} a & b \\ c & d \end{bmatrix} \cdot z = \frac{az + b}{cz + d}. \tag{1}$$

This action defines the Möbius transformations; one of these transformations, denoted by $\mathcal{M}$, is shown in Figure 3. However, because $-g \cdot z = +g \cdot z$, the group of Möbius transformations is the quotient group $\mathbf{PSL}(2, \mathbb{C} = \mathbf{SL}(2, \mathbb{C}/\{\pm Id\})$ in which matrices $\pm g$ are identified [11].

Now, if $f(z)$ is the image intensity function on the image plane, its projective transformations are the Möbius transformations that are given as follows:

$$\mathbf{PSL}(2, \mathbb{C}) \ni g = \begin{bmatrix} a & b \\ c & d \end{bmatrix} \longmapsto f\left(g^{-1} \cdot z\right) = f\left(\frac{dz - c}{-bz + a}\right). \tag{2}$$

The image of a small neighborhood of any point on the sphere $\mathcal{U}$ that does not contain N differs from $\sigma(\mathcal{U})$ in the image plane mainly by a dilation which is small for the viewing angle up to mid-periphery of about 60° and modest for the visual angle of 110° that restricts the binocular field limited by the nasal obstruction. Therefore, this conformal geometry preserves to a great degree the receptive fields and, hence, retinal illuminance as well as pixels, providing constructive properties for human vision [39, 41].

2.3 Geometry of the Conformal Eye

The group $\mathbf{SL}(2,\mathbb{C})$ with the action (1) is known as the Möbius group of holomorphic automorphisms of the complex structure on the Riemann sphere $\widehat{\mathbb{C}}$ [17]. The invariants under these automorphisms furnish *Möbius geometry* [14]. Further, $\mathbf{SL}(2,\mathbb{C})$ with the action (1) is the projective group of a one-dimensional complex geometry [6]. Thus, we have the isomorphism of the complex projective line and the Riemann sphere. This isomorphism means that the Riemann sphere synthesizes geometric and analytic (numerical) complex structures to provide a unique computational environment that is geometrically precise and numerically efficient.

The image plane does not admit a distance invariant under image projective transformations. Therefore, the camera's geometry does not possess a Riemann metric; for instance, there is no curvature. However, these transformations map circles to circles and, therefore, circles can play the role of geodesics. This fact makes the conformal model eye relevant to the intermediate-level vision computational aspects of natural scene understanding [39, 41].

3 The Projective Fourier Analysis

In the conformal eye model given by the Riemann sphere, the image can be represented in terms of the projective Fourier transform. The mathematical framework of this image representation is provided by Fourier analysis on the simplest semisimple group $\mathbf{SL}(2,\mathbb{C})$, the direction in well-understood representation theory of general semisimple groups initiated by Gelfand's school and completed by Harish-Chandra [15]—one of the greatest achievements of 20th-century mathematics.

The main idea of the Fourier analysis on groups is to decompose a space of functions defined on a set on which the group acts naturally in terms of the simplest homomorphisms of the group into the set of unitary linear operators on a Hilbert space. These simplest homomorphisms are the irreducible unitary representations of the group. In this framework, the generalized Fourier transform plays the same role on any group as the classical Fourier transform on the additive group of real numbers, where the irreducible unitary representations are homomorphisms between the additive group and the multiplicative group of complex numbers of modulus one (the circle group), given by the complex exponential functions one finds in the definition of the standard Fourier integral [27].

3.1 Projective Fourier Transform

The projective Fourier transform (PFT) was obtained in [36, 37] by restricting Fourier analysis on the group $\mathbf{SL}(2,\mathbb{C})$ to the image plane of the conformal model eye. The PFT of an image intensity function, $f(z)$, has the following expression:

$$\hat{f}(k,s) = \frac{i}{2}\int f(z)\left(\frac{z}{|z|}\right)^{-k}|z|^{-is}|z|^{-1}dzd\bar{z}, \tag{3}$$

where $(k,s)\in\mathbf{Z}\times\mathbf{R}$, and, if $z=x_1+ix_2$, then $(i/2)dzd\bar{z}=dx_1dx_2$. The functions $\Pi_{k,s}(z)=(z/|z|)^k|z|^{is}$ in (3) play the role of complex exponentials in the classical Fourier transform; their graphs for some values of k and s are shown in Figure 4.

In log-polar coordinates (u,θ) given by the complex logarithm,

$$\ln z = \ln re^{i\theta} = \ln r + i\theta = u + i\theta, \tag{4}$$

(3) takes on the form of the standard Fourier integral

$$\hat{f}(k,s) = \int f(e^{u+i\theta})e^{-i(us+\theta k)}e^u dud\theta. \tag{5}$$

In spite of the logarithmic singularity of log-polar coordinates, an image f is integrable on $\mathbb{C}\backslash\{0\}$. Therefore, we can remove a disk $|z|\leq r_a$ to regularize f such that $(u,\theta)\in(\ln r_a,\ln r_b)\times[0,2\pi)$. This is important in the derivation of the discrete PFT.

3.2 Discrete Projective Fourier Transform

The PFT in log-polar coordinates, the Fourier integral in (5), can be approximated by a double (M,N)-Riemann sum,

$$\hat{f}_{m,n} = \sum_{k=0}^{M-1}\sum_{l=0}^{N-1} f_{k,l}e^{u_k}e^{-i2\pi mk/M}e^{-i2\pi nl/N} \tag{6}$$

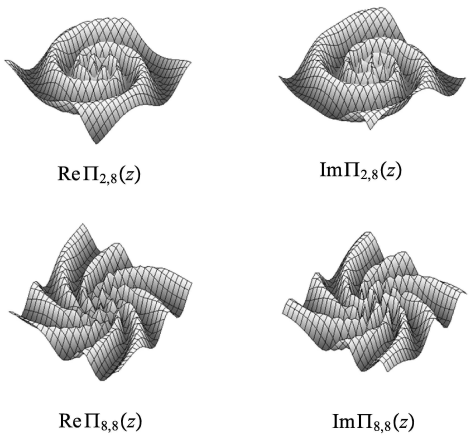

Figure 4: Graphs of the real and imaginary parts of the functions $\Pi_{k,s}$ for the selected values of k and s.

and its inverse,

$$\mathsf{f}_{k,l} = \frac{1}{MN}\sum_{m=0}^{M-1}\sum_{n=0}^{N-1}\hat{f}_{m,n}e^{-u_k}e^{i2\pi mk/M}e^{i2\pi nl/N}. \tag{7}$$

In these expressions, $f_{k,l} = (2\pi T/MN)f(e^{u_k}e^{i\theta_l})$ are image plane samples and $\mathsf{f}_{k,l} = (2\pi T/MN)\mathsf{f}(u_k,\theta_l)$ are log-polar samples where $T = \ln(r_b/r_a)$. I stress that $f(e^{u_k}e^{i\theta_l})$ differs from $\mathsf{f}(u_k,\theta_l)$; the first is defined on the image plane of the SE and the second is defined in cortical, log-polar coordinates. Both (6) and (7) can be computed efficiently by FFT.

Finally, by introducing $z_{k,l} = e^{u_k+i\theta_l}$ into (8) and (7) we arrive at (M,N)-point discrete projective Fourier transform (DPFT) and its inverse:

$$\hat{f}_{m,n} = \sum_{k=0}^{M-1}\sum_{l=0}^{N-1} f_{k,l}\left(\frac{z_{k,l}}{|z_{k,l}|}\right)^{-2\pi n/N}|z_{k,l}|^{-i2\pi mT+1} \tag{8}$$

and its inverse,

$$f_{k,l} = \frac{1}{MN}\sum_{m=0}^{M-1}\sum_{n=0}^{N-1}\hat{f}_{m,n}\left(\frac{z_{k,l}}{|z_{k,l}|}\right)^{2\pi n/N}|z_{k,l}|^{i2\pi mT-1}. \tag{9}$$

The covariant properties of the PFT are expressed as follows:

$$f'_{k,l} = \frac{1}{MN}\sum_{m=0}^{M-1}\sum_{n=0}^{N-1}\hat{f}_{m,n}\left(\frac{z'_{k,l}}{|z'_{k,l}|}\right)^{2\pi n/N}|z'_{k,l}|^{i2\pi mT-1}, \tag{10}$$

where $z'_{k,l} = g^{-1}\cdot z_{k,l},\ g\in\mathbf{SL}(2,\mathbb{C})$ and $f'_{k,l} = (2\pi T/MN)f(z'_{k,l})$. For the covariance to image transformations demonstration in image processing, see [35, 36, 37].

3.3 PFT and Retinotopy

How are the conformal eye model and the image representation in terms of PFT related to human vision? The human brain functions in physical space and receives information carried by light beams centrally projected onto the eyes' retinae and transduced by photoreceptors into electrochemical signals. After initial processing by the retinal circuitry, this visual information is mainly sent to the primary visual cortex (V1), where it produces specific retino-cortical mappings and forms input to other cortical areas [45]. This immensely complex processing decodes the environment from retinal stimulation and creates a neural representation of space [30], our subjective visual space.

The log-polar coordinates (4) approximate the retino-cortical mapping of the brain's visual pathway that topographically organizes visual and oculomotor brain areas [12]. Thus, whenever the retinal image changes as the effect of gaze rotations, the retinotopic map in V1 undergoes the corresponding changes that form the input for all next topographically organized areas that send feedback projections modulating the topographic maps.

The DPFT provides the data model for image representation that FFT can efficiently compute only in log-polar coordinates given by the complex logarithm $w = \ln(z)$. As mentioned before, the central foveal region $|z| \geq r_a$ must be removed to regularize the projective Fourier integral. The simplest, straightforward extension of the mapping $w = u + i\theta$, where $u = \ln(r)$ with $r > r_a$, to the region $0 \leq |z| \leq r_a$ can be obtained by taking linear extension of the radial part as follows

$$u = \frac{r - r_a}{r_a} + \ln r_a, \quad 0 \leq r \leq r_a,$$

which gives the model of retinotopy required when working with the DPFT.

This model differs from the often used in literature retinotopy model of V1. Moreover, the superior colliculus area [29, 33] described by the mappings $w = \ln(z \pm a) - \ln a$ where $a > 0$ removes logarithmic singularity and $\pm a$ indicates, for different signs, the left or right brain hemisphere. However, both complex logarithmic mappings modeling retinotopy give similar approximations for the peripheral region. In fact, for $|z| \ll a$, $\ln(z \pm a) - \ln a$ is approximately linear, while for $|z| \gg a$, it is dominated by $\ln z$.

In his model of retinotopy [29], Schwartz and his coworker proposed in [7] image processing in terms of the exponential chirp transform (ECT). The ECT is constructed by making the substitution:

$$(x, y) = (e^u \cos\theta, e^u \sin\theta) \tag{11}$$

in the standard 2D Fourier integral. Because the Jacobian of the transformation is translation-invariant, this substitution makes the ECT well adapted to translations in Cartesian coordinates. There is a clear dissonance between the nonuniform retinal image polar sampling grid and this Euclidean-shift invariance of the ECT.

On the other hand, the PFT is a genuine Fourier transform constructed from irreducible unitary representations of the group of image projective transformations. Further, the change of variables by $u = \ln r$ transforms the PFT into the standard Fourier integral, which is well regularized at the logarithmic singularity. Thus, the discrete PFT is computable by FFT in log-polar coordinates that approximate the retinotopy. The difference between (11) and (4) implies that the PFT does not experience the problem of exponentially-growing frequencies, like the ECT does, and for a band-limited original image, there is no difficulty with the Nyquist sampling condition in log-polar space, [36, 37].

Moreover, by the distinctive features of the complex logarithm $\ln z, \ln(e^{i\phi}z) = \ln z + i\phi, \ln(\rho z) = \ln z + \ln\rho$, the rotation and dilation transformations of an intensity function $f(e^u e^{i\theta})$ expressed in exp-polar coordinates correspond to simple translations of the log-polar image $\mathsf{f}(u, \theta)$ via $f(e^{i\phi}e^u e^{i\theta}) = f(e^u e^{i(\theta+\phi)}) = \mathsf{f}(u, \theta + \phi)$ and $f(\rho e^u e^{i\theta}) = f(e^{u+v}e^{i\theta}) = \mathsf{f}(u + v, \theta)$, where f and f were introduced in the previous section. These translation are very useful in the development of image identification and recognition algorithms. The Schwartz model of retinotopy, therefore, results in the destruction of these properties so critical to computational vision.

Further, there are also psychophysiological facts that support our modeling with DPFT. The accumulated evidence points to the fact that the fovea and periphery have different functional roles in vision and very likely involve different principles underlying image processing [31, 50]. Strikingly, the authors in [31] argue that the perceptual puzzle of the curveball, when batters often report that the flight of the ball undergoes a dramatic and nearly discontinuous shift in position as the ball nears the home plate, can be explained by the difference between the foveal and peripheral processing of the ball's image passing the boundary on the retina between these two regions.

Finally, sampling an image in log-polar coordinates conforms to the biological convergence of the retinal image sampled by photoreceptors on ganglion cells that send visual information to the visual cortex. The light carrying visual information about the external world impinged upon the retina is initially sampled by about 125 million photoreceptors. Then, after the retinal circuitry processes it, this visual information converges on about 1.5 million of ganglion cell axons that carry out the output from the eye to the brain's visual areas. In the numerical example [38], the original image has $262,144$ pixels, whereas this image sampled in log-polar coordinates contains only $2,664$ pixels. Thus, there are about 100 times fewer pixels in the sampled image in log-polar coordinates than in the original image.

Figure 5 shows a Matlab simulation of retinotopy with DPFT. In this simulation, the original San Diego harbor picture in Figure 5 (a) of the size 1024×1024 is resampled with 74 rings distributed exponentially and 128 sectors distributed uniformly (the exp-polar sampling). The inverse DPFT renders Figure 5 (c); both transforms, DPFT and its inverse, are computed in Matlab with FFT. Figure 5 (b) shows remapped pixel-by-pixel log-polar image in Figure 5 (c) to the Cartesian coordinates to represent the nonuniform sampling by the retina photoreceptors. The foveal region and the

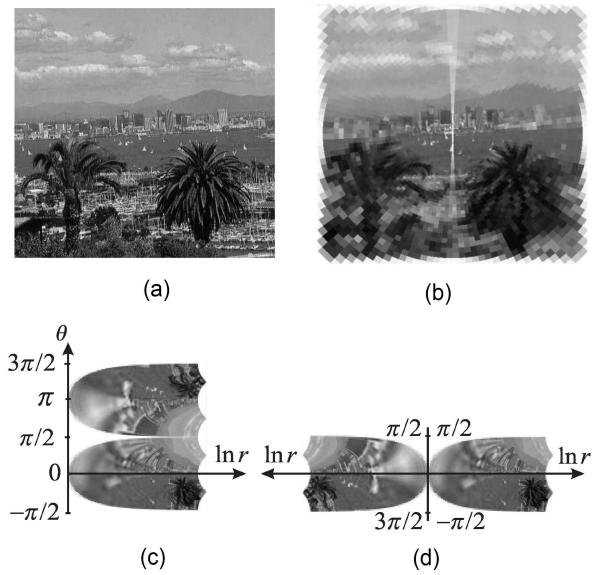

Figure 5: The model of retinotopy. See the text for the discussion.

vertical strip are excluded from regularizing PFT, which conforms to the different image processing in the foveal and extrafoveal regions and the split theory of hemispherical image representation.

According to the split theory, the foveal region has a functional split along the vertical meridian, with each half processed in a different brain hemisphere [19]. The global retinotopy, shown in Figure 5 (d), was simulated by the cut-and-paste transformation applied to Figure 5 (c). As it was demonstrated in [38], the global retinotopy can be done with FFT in log-polar coordinates.

I should note that in a robotic camera with anthropomorphic sensors, the retinal visual information represented by Figure 5 (b) will be given by the output from the silicon retina. Then, using the DPFT representation, this output data will be processed with FFT to emphasize brightness variations in retinal illuminance and rendered, also with FFT, as the log-polar (cortical) image.

4 Extension to AEs

In AE, an object's point projects to the point z_β on the image plane rotated by the angle β at the eye's rotation center C rather than to the point z in the image plane of SE, see Figure 6. I recall that β specifies the tilt of the effective lens such that the image plane in AE is parallel to the lens's equatorial plane. Because the visual axis is rotated by α degrees relative to the optical axis, the visual center on the image plane shifts from C to O where the visual axis intersects this plane. I need to find the transformation from z measured relative to C to z_β measured relative to O. Likewise, y_β is measured relative to O.

With this rule in mind, I use the right triangles $\Delta N y_\beta C$, $\Delta N y_\beta z_\beta$, $\Delta N y_\beta O$ and $\Delta N C z$ to get $|N y_\beta| = \cos\beta$, $z_\beta - y_\beta = \cos\beta \tan(\alpha - \beta + \varphi)$, $y_\beta = -\cos\beta \tan(\alpha - \beta)$ and $z = \tan(\alpha + \varphi)$. Then, using these relations in $z_\beta = (z_\beta - y_\beta) + y_\beta$ and standard trigonometric identities, we obtain

$$\begin{aligned} z_\beta &= \cos\beta\,[\tan(\alpha - \beta + \varphi) - \tan(\alpha - \beta)] \\ &= \cos\beta \left[\frac{z - \tan\beta}{z\tan\beta + 1} - \tan(\alpha - \beta)\right] \end{aligned}$$

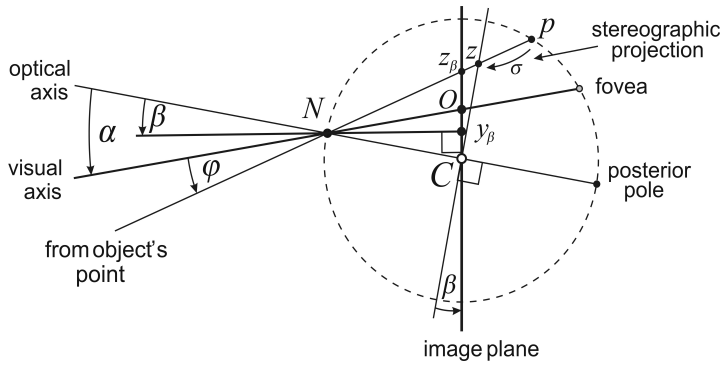

Figure 6: The extension of the CE model to the AE. The eyes asymmetry of optical components in the conformal eye model is represented as follows. The fovea's displacement from the posterior point by a constant angle $\alpha = 5.2^\circ$ gives the eyeball's global asymmetry. The lens-cornea system is given by the image plane tilted by angle β from the plane perpendicular to the optical axis and the north pole N of the unit sphere. β varies between people from -0.4° to 4.6° and N represents the nodal point. The imaging in this asymmetric CE is discussed in the text.

which can be written as

$$\begin{aligned} z_\beta &= \frac{z[1-\tan(\alpha-\beta)\tan\beta]\cos^{3/2}\beta - [\tan(\alpha-\beta)+\tan\beta]\cos^{3/2}\beta}{z[\tan\beta\cos^{1/2}\beta] + \cos^{1/2}\beta} \\ &= \begin{pmatrix} [1-\tan(\alpha-\beta)\tan\beta]\cos^{3/2}\beta & -[\tan(\alpha-\beta)+\tan\beta]\cos^{3/2}\beta \\ \tan\beta\cos^{1/2}\beta & \cos^{1/2}\beta \end{pmatrix} \cdot z \\ &= m_\beta \cdot z \end{aligned} \tag{12}$$

with $m_\beta \in \mathbf{SL}(2,\mathbb{C})$ given in terms of AE parameters. The expressions in (12) correct the result obtained in [41] where one of terms was left out.

If $z' = g \cdot z$, then $z_\beta = m_\beta \cdot z$ and $z'_\beta = m_\beta \cdot z'$ give $m_\beta \cdot z' = m_\beta g m_\beta^{-1} m_\beta \cdot z$ so that

$$z'_\beta = g_\beta \cdot z_\beta \quad \text{where} \quad g_\beta = m_\beta g m_\beta^{-1}. \tag{13}$$

This establishes the group $\mathbf{SL}(2,\mathbb{C})$ inner automorphism: $\mathbf{SL}(2,\mathbb{C}) \ni g \longmapsto m_\beta g m_\beta^{-1} \in \mathbf{SL}(2,\mathbb{C})$ established by

$$(g_1)_\beta (g_2)_\beta = (g_1 g_2)_\beta \tag{14}$$

and

$$(g_\beta)^{-1} = \left(g^{-1}\right)_\beta . \tag{15}$$

From the definition of image projective transformation, we can write,

$$T_g f(z) = f(m_\beta^{-1} m_\beta g^{-1} m_\beta^{-1} m_\beta \cdot z) = f_\beta(g_\beta^{-1} \cdot z_\beta) = T_{g_\beta} f_\beta(z_\beta)$$

where $f_\beta(z_\beta) = f(m_\beta^{-1} \cdot z_\beta) = f(z)$. The relation between g and g_β makes the diagram

$$\begin{array}{ccc} \widehat{\mathbb{C}} & \xrightarrow{g} & \widehat{\mathbb{C}} \\ {\scriptstyle m_\beta}\downarrow & & \downarrow{\scriptstyle m_\beta} \\ \widehat{\mathbb{C}} & \xrightarrow{g_\beta} & \widehat{\mathbb{C}} \end{array}$$

commutative such that m_β can be considered a coordinate transformation in the complex structure on $\widehat{\mathbb{C}}$. Since g and g_β have the same algebraic properties by (14) and (15), they behave geometrically in the same way. In another way of expressing the inner automorphism (13), it is to say that g and g_β are the same mappings in $\mathbf{SL}(2,\mathbb{C})$ expressed in different coordinates (geometer's point of view) or as the perceiving from a different perspective (physicist's point of view).

I summarize the symmetric CE and the asymmetric CE models as follows:

1. The image projective transformations the symmetric CE

$$f : D \longrightarrow \mathbb{R}, \quad g \in \mathbf{SL}(2,\mathbb{C})$$
$$f(z) \longrightarrow T_g f(z) = f(g^{-1} \cdot z).$$

2. The image projective transformation for the asymmetric CE

$$f_\beta : D' \longrightarrow \mathbb{R}, \quad g_\beta = m_\beta g m_\beta^{-1} \in \mathbf{SL}(2,\mathbb{C})$$
$$f_\beta(z') \longrightarrow T_{g_\beta} f_\beta(z') = f_\beta(g_\beta^{-1} \cdot z')$$

   where the AE parameters α and β define coordinates change m_β in (12).

To conclude this section, I can say that the result of tilting and translating the image plane does not affect the asymmetric CE's geometric and computational frameworks; this can be phrased as putting 'conformal glasses' on the symmetric CE.

5 Discussion

In [43, 44], the horopters closely resembling empirical horopters were constructed as conic sections in the binocular system with the AE model. The AE comprises two parameters: the fovea's anatomical displacement from the eyeball's posterior pole by angle α and the crystalline lens's tilt by angle β. In human eyes, the foveal displacement and the cornea asphericity contribute to the eye's optical aberrations that the lens' tilt is partially compensating.

It was demonstrated in [44] that the non-symmetrical distribution of retinal corresponding points, due to the natural eye's asymmetry, can be defined in the binocular system with the AEs in terms of the symmetrical distribution of the projected corresponding points into the AE's image plane. This geometric result suggests that one can fully describe the eye imaging function with the image plane of the AE, dispensing with the spherical retina.

To this end, I first considered the AE with $\alpha = \beta = 0$, the SE with a single refractive surface schematic eye. Following the tradition in vision science, I study three locations of the nodal point: the anatomically correct location at 0.6 cm anterior to the eye's rotation center, the pupil's location at the north pole of the unit sphere, and the location at the eye's rotation center. Only for the north pole location, two crucial properties of the eye model are satisfied. First, in addition to very good approximations for anthropomorphic binocular system's parameters, only for the nodal point placed at the north pole, it retains qualitative properties of the eye model with the correct location of the nodal point. Second, its image plane with the appended image of the north pole, i.e., the point at infinity, can be identified with the Riemann sphere. Thus, the image plane has conformal geometry. This eye model is referred to as the conformal eye.

Maybe unfamiliar to vision researchers, the automorphism group $\mathbf{SL}(2,\mathbb{C})$ of the Riemann sphere, which provides the projective image transformations of a rotating eye, has the subgroup $\mathbf{SU}(2)$ isomorphic to the group of unit quaternions [1] that have been used for a long time in vision science [49]. Moreover, this geometry provides a unique computational environment that is relevant to the intermediate-level vision computational aspects of natural scene understanding [39, 41].

Further, the conformal eye model established image representation in terms of the projective Fourier transform [35, 36, 37]—the model eye's intrinsic Fourier transform on the group of image projective transformations. This image representation changes covariantly with image transformations induced by eye movements. It is fast computable by FFT in log-polar coordinates that are known to approximate the retina-cortical mapping of the human brain's visual pathways [38, 41]. The image sampling in log-polar coordinates conforms to the biological convergence of the photoreceptors sampling the retinal image on the ganglion cells that send visual information to the visual cortex with about 100 times fewer pixels than in the original image [38].

Finally, the conformal eye model established first for the SE was extended to the AE. It corrects this extension proposed in [41] for the conformal camera. Therefore, the theory in [44] that integrates binocular vision with eye movement can be supported by the Riemann sphere's conformal geometry. Thus, this conformal AE model allows the image processing with the projective Fourier analysis developed by the author and reviewed in this article.

To conclude this discussion, I mention the future applications in the human binocular vision. The theory in [44] integrates binocular vision with eye movement. The importance of this becomes apparent when we realize that during natural viewing, the human eye's rotational speeds during saccades are as fast as $700^\circ/s$, with an acceleration exceeding $20,000^\circ/s^2$ [47]. Saccadic eye movements are performed about 3-4 times/s, meaning that the brain mainly acquires visual information during 3-4 brief fixations within a second. Thus, the visual information is acquired in a sequence of discrete snapshots, but we perceive a clear and stable world. In addition, we are not only able to execute smooth pursuit

eye movements that keep the foveae focused on a slowly moving object up to $100^\circ/s$; we also employ a combination of smooth pursuit and saccades to track an object moving unpredictably or moving faster than $30^\circ/s$ [48, 20]. By stabilizing the tracked object's image on the fovea, smooth pursuit eye movements (SPEMs) superimpose additional motion on the retinal images of the stationary background and the other moving objects.

The initial modeling of visual information during saccades and SPEM was carried out in [38, 42] for monocular vision. In [38], the perisaccadic predictive remapping of receptive fields by intended eye movement (via efference copy) [32] that is believed to maintain visual stability was modeled using the shift property of the projective Fourier transform in log-polar coordinates. This modeling remaps the current receptive fields to the future receptive fields before the incoming saccade takes them there. Also, it accounts for the observed in laboratory experiments the perisaccadic mislocalization of briefly flashed probes around of incoming saccade's target [26]. In [42], in the framework of the conformal eye model, the images of the stationary background sweeping across the retina during the pursuit of a small object moving in the front of the background were obtained in the initial image plane of a discrete sequence of small rotation angle approximation of the horizontal SPAM. Thus, modeling the visual information during smooth pursuit with the conformal eye can support anticipatory image processing. This anticipation can support the stability of visual information during tracking movements by an anthropomorphic camera needed for an autonomous robot's efficient interaction with the real world in real-time.

We saw that the basic feature underlying natural viewing is the occurrence of intricate dynamic disparities that are processed to maintain our clear vision that appears continuous and stable. In this regard, the theory in [44] provides the binocular conics' transformations during eye movement and, therefore, allows the monocular vision stability in [38, 42] to be extended to the binocular framework.

APPENDIX

A Projecting Retina into Image Plane in SE Model

I demonstrate here that the projections of circles (the receptive fields) on the retina to the image plane of the SE model are conics as claimed before in Figure 1. The planar intersection of this SE model is abstracted in the following figure.

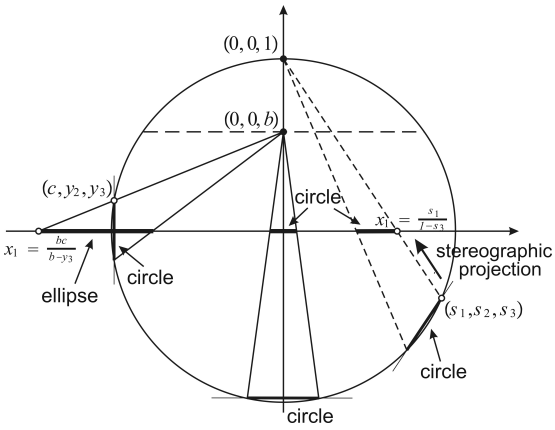

Figure 7: The SE model's planar intersection. The projection through the nodal point $(0, 0, b)$ from the retina to the image plane is shown with solid rays. In general, it maps circles in the retina to conic sections in the image plane. The stereographic projection is depicted with dashed rays. It maps circles in the retina (located below the horizontal gashed line) onto circles in the image plane.

The projection from the north pole $(0, 0, 1)$ (the eye's pupil) of the sphere to the image plane passing through the sphere's center is the stereographic projection. It maps circles in the sphere (the intersection of the sphere with a plane) that do not contain the north pole to the circles in the plane, see Figure 3. I will demonstrate that the projections from the nodal point $(0, 0, b)$ of the retina's circles into the image plane are conic sections. Moreover, I estimate the eccentricity range of the ellipses (the ratio of their axes) in the image plane region subtended the visual angle at the nodal point of 110° for $b = 0.6$.

The points (c, y_2, y_3) on the sphere $y_1^2 + y_2^2 + y_3^2 = 1$ form the circle $y_2^2 + y_3^2 = 1 - c^2$. The points of the circle with $c < 1$ but close to 1 projected through $(0, 0, b)$ to the image plane are

$$x_1 = \frac{bc}{b - y_3}, \;\; x_2 = \frac{by_2}{b - y_3} \tag{16}$$

These equations are solved for y_2 and y_3,

$$y_2 = \frac{cx_2}{x_1}, \;\; y_3 = b - \frac{bc}{x_1} \tag{17}$$

and substituted into the circle $y_2^2 + y_3^2 = 1 - c^2$ yields the equation

$$\frac{c^2x_2^2}{x_1^2} + \left(b - \frac{bc}{x_1}\right)^2 = 1 - c^2.$$

This equation can be rewritten as

$$\frac{b^2 + c^2 - 1}{b^2c^2(1 - c^2}\left(x_1 - \frac{b^2c}{b^2 + c^2 - 1}\right)^2 + \frac{b^2 + c^2 - 1}{b^2(1 - c^2}x_2^2 = 1 \tag{18}$$

The equation (18) is an ellipse if $c^2 > 1 - b^2$ and $c^2 < 1$, that is, if

$$c \in \left(-1, -\sqrt{1 - b^2}\right) \cup \left(\sqrt{1 - b^2}, 1\right). \tag{19}$$

Further, the equation (18) is a parabola for $c = \pm\sqrt{1 - b^2}$ and hyperbola for $c \in \left(-\sqrt{1 - b^2}, \sqrt{1 - b^2}\right)$.

Before I estimate the ellipses shapes, we first note that the circle $y_1^2 + y_2^2 = 1 - d^2$ in the sphere is projected through $(0, 0, b)$ to a circle in the image plane because the symmetry of projection: the center of this circle on the retina is at $(0, 0, d)$ and the projection is from $(0, 0, b)$, cf. Figure 7. Now, the ellipses axes ratios in the image plane region that is subtending visual angle 110° are in the interval $(0.7, 1)$. The ration 1 is corresponding to a circle.

References

[1] Altmann, S.L.: Rotations, Quaternions and Double Groups. Oxford University Press, Oxford and NY 1986.

[2] Amigo, G. The mathematical treatment of horopter data obtained with the eyes in asymmetric convergence, Opt. Acta 1965, 12, 305–315.

[3] Artal, P. Optics of the eye and its impact in vision: a tutorial, Adv. Opt. Photon 2014, 6, 340–367.

[4] Atchison, D.A. and Thibos, L.N. Optical models of the human eye, Clin. Exp. Optom. 2016, 99, 99–106.

[5] Atchison, D.A. Optical models for human myopic eyes. Vision Res. 2006, 46, 2236–2250.

[6] Berger, M. Geometry I; Springer: NY 1987.

[7] Bonmassar, G.; Schwartz, E.L. Space-variant Fourier analysis: The Exponential Chirp transform. IEEE Trans. Pattern Anal. 1997, 19, 1080–1089.

[8] Chang, Y.;Wu, H.-M.; Lin, Y.-F. The axial misalignment between ocular lens and cornea observed by MRI (I)—At fixed accommodative state. Vision Res. 2007, 47, 71–84

[9] Charman, W,N. The eye in focus: accommodation and presbyopia. Clin. Exp. Optomet. 2008, 91, 207–225. doi: 10.1111/j.1444-0938.2008.00256.x

[10] Demer, J.L. Current concepts of mechanical and neural factors in ocular motility. Curr. Opin. Neurobiol. 2006, 19, 4–13. doi: 10.1097/01.wco.0000198100.87670.37

[11] Durbin, J.R. Modern Algebra. An Introduction Ed. 5; Wiley, NJ 2005.

[12] Engel, S.A.; Glover, G.H.; Wendell, B.A. Retinotopic organization in human visual cortex and the spatial precision of MRI. Cerabral Cortex 1997, 7, 181–192.

[13] Gao, Z., Guo, H., and Chen, W. Initial tension of the human extraocular muscles in the primary eye position. J. Theor. Biol. 2014, 353, 78–83. doi: 10.1016/j.jtbi.2014.03.018

[14] Henle, M. Modern Geometries. The Analytical Approach; Prentice Hall: Upper Saddle River, NJ 1997.

[15] Herb, R.A. An Elementary Introduction to Harish-Chandra's Work. In Mathematical Legacy of Harish-Chandra—A Celebration of Representation Theory and Harmonic Analysis; Doran, R.S., Varadarajan, V.S., Eds.; AMS: Providence, RI 2000, Volume 68, pp. 59–75.

[16] Holladay, J.T. Quality of vision: essential optics for cataract and refractive surgeon. Slack Inc., Thorofare, NJ 2007.

[17] Jones, G.; Singerman, D. Complex Functions; Cambridge University Press: Cambridge 1987.

[18] Koenderink, J. Fundamentals of bicentric perspective, in Future Tendencies in Computer Science, Control and Applied Mathematics, Vol. 653, Lecture Notes in Computer Science, eds A. Bensoussan and J. P. Verjus, Berlin, Heidelberg: Springer 1992, 233–251. doi: 10.1007/3-540-56320-2-62.

[19] Martin, C.D., Thierry, G., Dmonet, J-F., Roberts, M., and Nazira, T. ERP evidence for the split fovea theory. Brain Res. 2007, 1185, 212-220.

[20] Meyer, C. H., Lasker, A. G., and Robinson, D. A. The upper limit of human smooth pursuit velocity. Vision Res. 1985, 25, 561–563. doi: 10.1016/0042-6989(85)90160-9

[21] Needham, T. Visual Complex Analysis; Oxford University Press: New York, NY 2002.

[22] Ogle, K.N. Analytical treatment of the longitudinal horopter. J. Opt. Soc. Am. 1932, 22, 665–728.

[23] Ogle, K.N. Precision and validity of stereoscopic depth perception from double image, J. Opt. Soc. Am. 1953, 41, 906–913.

[24] Polans, J., Jaeken, B., McNabb, R.P., Artal, P., and Izatt, J.A. Wide-field optical model of the human eye with asymmetrically tilted and decentered lens that reproduces measured ocular aberrations. Optica 2015, 2, 124-134.

[25] Radhakrishnan, H. and Charman, W. Changes in astigmatism with accommodation. Ophthal. Physiol. Opt. 2007, 27, 275–280. doi: 10.1111/j.1475-1313.2007.00474.x

[26] Ross J, MorroneM C, GoldbergM E, and Burr, D.C. Changes in visual perception at the time of saccades. Trends Neurosci. 2001, 24:113–121

[27] Sally, P.J., Jr. Harmonic analysis and group representations. In Studies in Harmonic Analysis; Ash, J.M., Ed.; Mathematical Association of America: Washington, DC 1976, Volume 13 pp. 224–256.

[28] Schreiber K.M., Tweed D.B., and Schor C.M. The extended horopter: Quantifying retinal correspondence across changes of 3D eye position. Journal of Vision 2006, 6, 64–74.

[29] Schwartz, E.L. Computational anatomy and functional architecture of striate cortex. Vision Res. 1980, 20, 645–669.

[30] Sereno, A. B., and Lehky, S. R. Population coding of visual space: comparison of spatial representations in dorsal and ventral pathways. Front. Comput. Neurosci. 2011, 4,159. doi: 10.3389/fncom.2010.00159

[31] Shapiro, A.; Lu, Z.-L.; Huang, C.-B.; Knight, E.; Ennis, R. Transitions between Central and Peripheral Vision Create Spatial/Temporal Distortions: A Hypothesis Concerning the Perceived Break of the Curveball. PLoS ONE 2010, 5, doi:10.1371/journal.pone.0013296.

[32] Sommer, M. A., Wurtz, R. H.: Brain circuits for the internal monitoring of movements. Annu. Rev. Neurosci. 2008, 31, 317-338.

[33] Tabareau, N.; Bennequin, N.D.; Berthoz, A.; Slotine, J.-J. Geometry of the superior colliculic mapping and efficient oculomotor computation. Biol. Cybern. 2007, 97, 279–292.

[34] Tabernero, J., Benito, A., Alcón,E., and Artal, P. Mechanism of compensation of aberrations in the human eye. J. Opt. Soc. Am. A 2007, 24, 3274–3283.

[35] Turski, J. Projective Fourier analysis for patterns. Pattern Recogn. 2000, 33, 2033-2043

[36] Turski, J. Geometric Fourier Analysis of the Conformal Camera for Active Vision. SIAM Rev. 2004, 46, 230-255

[37] Turski, J. Geometric Fourier Analysis for Computational Vision. J Fourier Anal Appl. 2005, 11, 1-23

[38] Turski, J. Robotic Vision with the Conformal Camera: Modeling Perisaccadic Perception. J Robotics 2010, doi:10.1155/2010/130285, 1-16

[39] Turski, J. Imaging with the Conformal Camera, Proc. IPCVIPR., Vol. II 2012, CSREA Press.

[40] Turski, J. On binocular vision: The geometric horopter and cyclopean eye. Vision Research 2016, 119,73–81. doi:10.1016/j.visres.2015.11.001

[41] Turski, J. The Conformal Camera in Modeling Active Binocular Vision. Symmetry 2016, 08;8:1–22.

[42] Turski, J. Modeling active vision during smooth pursuit of a robotic eye. Electron. Imaging 2016, 1–8. doi: 10.2352/ISSN.2470-1173.2016.10.ROBVIS-391

[43] Turski, J. Binocular system with asymmetric eyes. Journal of the Optical Society of America A 2018, 35, 1180–1191. doi:10.1364/JOSAA.35.001180

[44] Turski, J. A Geometric Theory Integrating Human Binocular Vision with Eye Movement. Front. Neurosci. 2020, 14:555965. doi: 10.3389/fnins.2020.555965

[45] Wandell, B. A., Dumoulin, S. O., and Brewer, A. A. Visual field maps in human cortex. Neuron 2007, 56, 366–383. doi:10.1016/j.neuron.2007. 10.012

[46] Tyler, C. W. Binocular vision. In W. Tasman & E. A. Jaeger (Eds.). Duane's foundations of clinical ophthalmology (Vol. 2). Philadelphia: J.B. Lippincott. 2004.

[47] Waitzman, D. "Oculomotor systems and control," in Conn's Translational Neuroscience, ed P. Conn (London; San Diego, CA; Cambridge; Oxford: Academic Press) 2016, 439–465. doi: 10.1016/B978-0-12-802381-5.00032-4

[48] Westheimer, G. Eye movement responses to a horizontally moving visual stimulus. Arch. Ophthalmol. 1954, 52, 932–941. doi: 10.1001/archopht.1954.00920050938013

[49] Westheimer, G. Kinematics of the eye. Journal of the Optical Society of America 1957, 47, 961-974.

[50] Xing, J. and Heeger, D.J. Center-surround interaction in foveal and peripheral vision. Vis. Res. 2000, 40, 3065–3072.